UCLA

UCLA Previously Published Works

Title

Human perivascular stem cell-based bone graft substitute induces rat spinal fusion.

Permalink

https://escholarship.org/uc/item/19209322

Journal

Stem Cells Translational Medicine, 3(10)

ISSN

2157-6564

Authors

Chung, Choon

James, Aaron

Asatrian, Greg

et al.

Publication Date

2014-10-01

DOI

10.5966/sctm.2014-0027

Peer reviewed

eScholarship.org Powered by the California Digital Library
University of California

STEM CELLS TRANSLATIONAL MEDICINE®

TISSUE ENGINEERING AND REGENERATIVE MEDICINE

Human Perivascular Stem Cell-Based Bone Graft Substitute Induces Rat Spinal Fusion

CHOON G. CHUNG,[a] AARON W. JAMES,[a,b,c] GREG ASATRIAN,[a] LE CHANG,[a] ALAN NGUYEN,[a] KHOI LE,[a] GEORGINA BAYANI,[a] ROBERT LEE,[a] DAVID STOKER,[d] XINLI ZHANG,[a] KANG TING,[a,b,e] BRUNO PÉAULT,[b,f] CHIA SOO[b,e,g]

Key Words. Perivascular stem cell • Adventitial cell • Mesenchymal stem cell • Osteogenesis • Pericyte • Tissue engineering

ABSTRACT

Adipose tissue is an attractive source of mesenchymal stem cells (MSCs) because of its abundance and accessibility. We have previously defined a population of native MSCs termed perivascular stem cells (PSCs), purified from diverse human tissues, including adipose tissue. Human PSCs (hPSCs) are a bipartite cell population composed of pericytes (CD146+CD34−CD45−) and adventitial cells (CD146−CD34+CD45−), isolated by fluorescence-activated cell sorting and with properties identical to those of culture identified MSCs. Our previous studies showed that hPSCs exhibit improved bone formation compared with a sample-matched unpurified population (termed stromal vascular fraction); however, it is not known whether hPSCs would be efficacious in a spinal fusion model. To investigate, we evaluated the osteogenic potential of freshly sorted hPSCs without culture expansion and differentiation in a rat model of posterolateral lumbar spinal fusion. We compared increasing dosages of implanted hPSCs to assess for dose-dependent efficacy. All hPSC treatment groups induced successful spinal fusion, assessed by manual palpation and microcomputed tomography. Computerized biomechanical simulation (finite element analysis) further demonstrated bone fusion with hPSC treatment. Histological analyses showed robust endochondral ossification in hPSC-treated samples. Finally, we confirmed that implanted hPSCs indeed differentiated into osteoblasts and osteocytes; however, the majority of the new bone formation was of host origin. These results suggest that implanted hPSCs positively regulate bone formation via direct and paracrine mechanisms. In summary, hPSCs are a readily available MSC population that effectively forms bone without requirements for culture or predifferentiation. Thus, hPSC-based products show promise for future efforts in clinical bone regeneration and repair. STEM CELLS TRANSLATIONAL MEDICINE *2014;3:1231–1241*

INTRODUCTION

Skeletal diseases, whether congenital or acquired, are one of the most frequent and costly medical conditions and are expected to increase as the U.S. population continues to age. The escalating burden of musculoskeletal diseases is depicted through its rising cost in the U.S.; in 1992, the total cost of musculoskeletal diseases incurred $149.4 billion, whereas in 2004, the cost had risen to $849 billion, equivalent to 7.7% of the gross domestic product [1, 2]. Specifically, spinal fusion procedures have become ubiquitous, with more than 350,000 spinal fusions performed per annum in the U.S., a 200% increase over the past decade [3–7]. Currently, autogenous bone grafting is considered the gold standard for skeletal reconstruction. However, limited availability and significant complications (such as donor site morbidity, increased operative and recovery time, and pain) have prompted the search for safer and more effective alternatives [8–10]. Mesenchymal stem cells (MSCs) are multipotent stromal cells capable of regenerating mesenchymal tissues. Well studied for their application in skeletal engineering, bone marrow mesenchymal stem cells (BMSCs) are the main source of MSCs for bone regeneration [11–13]. However, distinct disadvantages exist for the use of BMSCs, such as limited autogenous supply, requirement for culture-based derivation and expansion, and reduced cellular activity in aged or osteoporotic patients [14, 15].

Another promising source of MSCs is adipose tissue, because this source is highly accessible and abundant. Adipose-derived stem cells demonstrate clear advantages over BMSCs in availability, yet in vitro cell culture increases the risk of immunogenicity, genetic instability, and infection [16–21]. To circumvent these risks, interest has risen in the use of the noncultured stromal vascular fraction (SVF) of adipose tissue among such companies as IntelliCell (New York, NY, http://www.intellicellbiosciences.com) and Cytori Therapeutics, Inc. (San Diego, CA, http://www.cytori.com). However, SVF is well recognized to be a heterogeneous population including nonstem cells,

[a]Dental and Craniofacial Research Institute and Section of Orthodontics, School of Dentistry, [b]UCLA and Orthopaedic Hospital Department of Orthopaedic Surgery and the Orthopaedic Hospital Research Center, [c]Department of Pathology and Laboratory Medicine, [e]UCLA Operation Mend, and [g]Division of Plastic and Reconstructive Surgery, Department of Surgery, University of California, Los Angeles, Los Angeles, California, USA; [d]Marina Plastic Surgery Associates, Marina del Rey, California, USA; [f]Center for Cardiovascular Science and MRC Center for Regenerative Medicine, University of Edinburgh, Edinburgh, United Kingdom

Correspondence: Kang Ting, D.M.D., D.Med.Sc., Section of Orthodontics, School of Dentistry, University of California, Los Angeles, 10833 Le Conte Avenue, CHS 30-117, Los Angeles, California 90095, USA. Telephone: 310-713-9979; E-Mail: kting@ucla.edu; or Bruno Péault, Ph.D., Department of Orthopaedic Surgery, University of California, Los Angeles, 615 Charles E. Young Drive South, Room 410, Los Angeles, California 90095, USA. Telephone: 310-794-1339; E-Mail: bpeault@mednet.ucla.edu; or Chia Soo, M.D., F.A.C.S., Division of Plastic and Reconstructive Surgery, Department of Orthopaedic Surgery, University of California, Los Angeles, 675 Charles E. Young Drive South, MRL 2641A, Los Angeles, California 90095-1579, USA. Telephone: 310-794-5479; E-Mail: bsoo@ucla.edu

Received February 12, 2014; accepted for publication June 16, 2014; first published online in SCTM *EXPRESS* August 25, 2014.

©AlphaMed Press
1066-5099/2014/$20.00/0

http://dx.doi.org/10.5966/sctm.2014-0027

such as inflammatory, hematopoietic, and endothelial cells, which results in unreliable bone formation [22–24]. With these drawbacks of currently available MSC sources, there exists a clinical need for a reliable source of MSC with proven safety, purity, identity, and efficacy.

Our laboratory has identified and isolated perivascular stem cells (PSCs) from multiple vascularized tissues using a fluorescence-activated cell sorting (FACS) method [25–29]. PSCs are identified by their cell surface markers and include pericytes from microvessels and capillaries (which are CD34−, CD146+, CD45−) and adventitial cells from larger arteries and veins (which are CD34+, CD146−, CD45−) [30]. PSCs exhibit the characteristic surface markers and clonal multilineage differentiation potential of MSCs [25–29]. The evidence supporting the use of human perivascular stem cells (hPSCs) for bone tissue engineering is based on our prior studies: firstly, human pericytes derived from pancreas (and other organs) exhibit robust in vitro osteogenic differentiation and intramuscular bone formation and angiogenesis [31]. Next, adipose-derived hPSCs form significantly increased intramuscular bone compared with patient-matched unpurified cells and demonstrate in vivo trophic and angiogenic effects [32, 33]. Lastly adipose-derived hPSCs exhibited improved calvarial bone defect healing as compared with unsorted SVF [34].

In the present study, we sought to translate the regenerative potential of hPSCs to a functionally demanding rat spinal fusion model. We observed that hPSC treatment induces endochondral bone formation and rigid mechanical fixation of the lumbar spine in rats, as compared with an acellular control.

Materials and Methods

Isolation of Human SVF From Human Lipoaspirate and Purification of hPSC From Human SVF

Human lipoaspirate was collected from cosmetic liposuction patients (n = 4 patients). The whole lipoaspirate was stored at 4°C before processing and processed within 48 hours of collection. The human stromal vascular fraction (hSVF) was obtained by collagenase digestion as previously described [30]. Briefly, an equal volume of phosphate-buffered saline (PBS) was added to dilute the lipoaspirate. The mixture was then digested with Dulbecco's modified Eagle's medium containing 3.5% bovine serum albumin (Sigma-Aldrich, St. Louis, MO, http://www.sigmaaldrich.com) and 1 mg/ml collagenase type II for 70 minutes under agitation at 37°C. Next, adipocytes were separated and excluded by centrifugation. The processed hSVF was suspended in red cell lysis buffer (155 mM NH_4Cl, 10 mM $KHCO_3$, and 0.1mM EDTA) and incubated for 10 minutes at room temperature. The incubated hSVF was resuspended in PBS, and 4′,6-diamidino-2-phenylindole (DAPI; Invitrogen, Carlsbad, CA, http://www.invitrogen.com) was added to exclude dead cells and filtered through a 70-μm cell filter. The resulting hSVF was immediately processed for hPSC purification. The number of live cells was calculated by trypan blue staining. Patient demographics for the lipoaspirate used, including gender, age, and anatomic location is presented in supplemental online Table 1.

Purification of hPSCs From hSVF

hPSCs were purified from the isolated hSVF by FACS as previously described [30, 34]. Briefly, hSVF was incubated at 4°C for 15 minutes in dark surroundings with the following conjugated antibodies: anti-CD34-phycoerythrin (Dako, Glostrup, Denmark, http://www.dako.com), anti-CD45-allophycocyanin (Santa Cruz Biotechnology Inc., Santa Cruz, CA, http://www.scbt.com), and anti-CD146-fluorescein isothiocyanate (AbD Serotec, Raleigh, NC, http://www.ab-direct.com). Next, DAPI was added to remove any nonviable cells from the mixture. The resulting cell population was processed on the FACS Aria cell sorter (BD Biosciences, San Diego, CA, http://www.bdbiosciences.com). Consequently, two populations of cells were sorted according to their cell surface markers to constitute hPSCs: distinct pericytes (CD34−, CD146+, CD45−) and adventitial cells (CD34+, CD146−, CD45−) [25, 28, 29].

Implant Preparation

Demineralized bone matrix (DBX) putty (300 μl per side; ovine source; Musculoskeletal Transplant Foundation, Edison, NJ, https://www.mtf.org), a combination of morselized cortical and cancellous bone chips mixed with sodium hyaluronate, was used as a scaffold for cell delivery. Defined numbers of cells were suspended in 50 μl of PBS and mixed mechanically with DBX particles. Cell numbers and concentrations were based on previously published data [32] and are fully described in Table 1. Implants were kept on ice prior to in vivo implantation.

Animal Model and Surgical Procedures

Athymic rats were used to prevent immune response to human cells. All animals were treated with postoperative medications of buprenorphine for 48 hours and trimethiprim/sulfamethoxazole for 10 days, for pain management and prevention of infection, respectively. Animals were housed and experiments were performed in accordance with the guidelines of the Chancellor's Animal Research Committee for Protection of Research Subjects at the University of California, Los Angeles.

Posterolateral lumbar spinal fusion was performed on 8-week-old athymic rats (n = 23) as previously described [35]. Rats were anesthetized using isoflurane (5% induction, 2%–3% maintenance). Posterior midline incisions were made over the caudal portion of the lumbar spine, and two separate fascial incisions were made 4 mm bilaterally from the midline. Blunt muscle splitting technique was used lateral to the facet joints to expose the transverse processes of L4 and L5 lumbar spines. The processes were then decorticated using a low speed burr under regular irrigation with sterile saline solution to cool the decortication site and maintain a clean surface for implantation. Next, the treatment material was delivered via a scaffold, implanted between the transverse processes bilaterally into the paraspinal muscle bed. Finally, the fasciae and skin were each closed using a simple continuous technique with 4-0 Vicryl sutures (Ethicon Endo-Surgery, Blue Ash, OH, http://http://www.ethicon.com). Rats were sacrificed 4 weeks postsurgery via CO_2 overdose, and the spines were harvested for analysis.

Manual Palpation

At 4 weeks postimplantation, the lumbar spine specimens were retrieved en bloc. Manual palpation was performed to evaluate the reduction of motion between the lumbar spines of rats postharvest. The samples were palpated by three blinded observers and scored on a scale of 1–5 by application of flexion and extension forces manually against the L4 and L5 vertebrae as previously described [36]. The scoring criteria were as follows: 1 indicates

©AlphaMed Press 2014

Table 1. Cell numbers and concentrations

Treatment group[a]	Sample size (*n*)	Concentration (cells per milliliter)
Control	5	0
0.15×10^6 hPSCs	6	0.25×10^6
0.50×10^6 hPSCs	5	0.83×10^6
1.50×10^6 hPSCs	6	2.50×10^6

[a]Treatment groups for study. Note that 300 μl of demineralized bone matrix scaffold was implanted per side.
Abbreviation: hPSC, human perivascular stem cell.

motion between vertebrae, with no bone mass formation; 2 indicates motion with a unilateral bony mass; 3 indicates motion with bilateral bony masses; 4 indicates no motion between vertebrae, with moderate bilateral bone masses bridging transverse processes; and 5 indicates no motion, with abundant bilateral bone masses bridging transverse processes. Scores of 4 or above were considered to be reflective of spinal fusion.

High-Resolution Quantitative Micro-Computed Tomography Analysis

In preparation for micro-computed tomography (micro-CT) imaging, all samples were stored in 4% paraformaldehyde for 48 hours. Samples were scanned using high-resolution micro-CT (Skyscan 1172F; Skyscan, Kontich, Belgium, http://www.skyscan.be) at an image resolution of 20 μm (55 kV and 181 mA radiation source, using a 0.5-mm aluminum filter) and analyzed using DataViewer, Recon, CTAn, and CTVol software provided by the manufacturer. All quantitative and structural parameters follow the nomenclatures described by the American Society for Bone and Mineral Research Nomenclature Committee [37].

Three-dimensional (3D) data analysis was carried out by manually drawing polygonal regions of interest (ROIs) designed to encircle the newly formed bone mass between the L4 and L5 transverse processes. Regions of interest were designed to include the implant material and newly formed bone but exclude pre-existing bone structures. Analyses included bone mineral density, bone volume/tissue volume (bone volume density), trabecular thickness, trabecular spacing, and trabecular number. A threshold value range of 60–120 was selected to best represent the newly formed bone using a global thresholding technique [37].

Biomechanical Analysis (Finite Element Analysis)

To determine three-dimensional quantities, such as the subtle changes in microstructural and mechanical properties of bone, we chose to use computerized biomechanical simulation. Direct experimental assessments are plagued with large errors and uncertain significance [38–40]. Therefore, to more accurately evaluate the biomechanical properties of fusion in the bilateral bone bridge, we used finite element models to simulate real mechanical tests. In order to accomplish this, micro-CT images were converted to DICOM files using SkyScan Dicom Converter software (DicomCT application; Skyscan 1172F, Skyscan). Macro- and microsimulations were performed to evaluate the biomechanical properties of the fusion sites. First, tetrahedral three-dimensional mesh models were created by drawing a ROI to isolate L4 and L5 lumbar vertebrae and their respective newly formed fusion masses, using ScanIP software (Simpleware Ltd., Exeter, U.K., http://www.simpleware.com). Second, tetrahedral 3D cube shaped mesh models with dimensions of 2 mm $\times$ 2 mm $\times$ 2 mm were created from both the right and left sides of newly formed bone of the fusion site, which were segmented using Mimics' intensity threshold (range, 1,250–4,095) in Mimics software (version 16.0; Materialise, Leuven, Belgium, http://www.materialise.com). 3-matic (version 8.0; Materialise) was used to remesh these 3D mesh models with a shape quality threshold of 0.3 height/area, and a maximum triangle edge length of 0.1 mm. Following remeshing, the 3D cube models had an average of 110,000 elements. Finite element analyses were performed using the ABAQUS software (version 6.12; Dassault Systèmes, Velizy-Villacoublay, France, http://www.3ds.com). Material properties of cancellous bone were considered to be isotropic, homogeneous, and linearly elastic with an elastic modulus of 3.5 GPa and a Poisson's ratio of 0.25 [41]. Boundary conditions constrained all displacements and rotations on the lower (caudal) border nodes of the L5 vertebral body and 3D cube models. Next, we applied a uniform compressive stress force of 0.5 MPa on the superior surface of the L4 vertebral body and 3D cube models to reproduce human intradiscal pressure experienced in relaxed standing to the upper (rostral) border nodes of the L4 vertebral body [42]. Finally, the mean von Mises stress experienced of the samples were analyzed.

Histology and Immunohistochemistry Analysis

After micro-CT analysis, samples were decalcified using 19% EDTA and embedded in paraffin. Hematoxylin and eosin (H&E) and Masson's trichrome staining was performed on deparaffinized sections following standard protocols [31]. Next, immunohistochemical staining was performed with primary antibodies against both human and rat major histocompatibility complex (MHC) class I antigens (Santa Cruz Biotechnology), osteocalcin (OCN) (Santa Cruz Biotechnology), and bone sialoprotein (BSP) (Chemicon, Temecula, CA, http://www.chemicon.com) using the ABC (Vector Laboratories, Burlingame, CA, http://www.vectorlabs.com) method. Immunohistochemistry was performed after paraffin slices were deparaffinized, dehydrated, rinsed, and incubated with 3% H_2O_2 for 20 minutes. All sections were then blocked with 0.1% bovine serum albumin in PBS for 1 hour. At a dilution of 1:100, primary antibodies were added to each section and incubated at 37°C for 1 hour or overnight at 4°C. Images were obtained on an Olympus (Center Valley, PA, http://www.olympusamerica.com) BX51 fluorescence microscope. For selected experiments, bone formation was quantified by blinded histomorphometric analyses using H&E staining and Photoshop (Adobe Systems Inc., San Jose, CA, http://www.adobe.com) quantification as expressed by bone area/total implant tissue area. Additionally, selected immunohistochemistry samples had semiquantifications of positive staining performed using the magic wand tool in Adobe Photoshop with a tolerance setting of 30. Semiquantification of positive staining in OCN- and BSP-stained samples was also performed. Finally, to investigate the origin of the differentiated osteoblasts and osteocytes, species specific quantification of positive staining of MHC was performed.

Bone Labeling and Histomorphometric Analysis

To visualize the bone-forming activity of each treatment group, animals from each groups were divided into two different in vivo

 ©AlphaMed Press 2014

labeling groups for bone histomorphometric analysis: (a) calcein-calcein intraperitoneal injections and (b) calcein-demeclocycline intraperitoneal injections. Animals were injected with calcein (20 mg/kg) 9 days prior to sacrifice and followed by an identical dose of either calcein or demeclocycline (6 mg/kg) 2 days before sacrifice. The time interval between the 2 injections was 1 week. Images were obtained using an Olympus BX51 fluorescence microscope. To compensate for the irregularity of DBX scaffold implants, instead of measuring the length between the two intervals, semiquantification was performed as a relative percentage of positive fluorescence over control value.

Statistical Analysis

Statistical analysis was performed using the appropriate analysis of variance to analyze more than two groups, followed by post hoc Tukey's test analysis between specific groups. $p < .05$ (*) and $p < .01$ (**) were considered to be significant.

RESULTS

Evaluation of Spinal Fusion Using Manual Palpation

At 4 weeks post implantation, flexion/extension forces were used to evaluate gross intervertebral motion. Fusion was graded using a 5-point scale, as previously described [41, 43], with a score of 4 or greater considered fused. hPSC treatment resulted in significantly increased spinal fusion rates in comparison with the acellular control. All three dosages of hPSCs (0.15×10^6, 0.5×10^6, and 1.5×10^6) resulted in fusion rates of 100%, 80%, and 100%, respectively, compared with 20% fusion in the acellular control group (Fig. 1). In summary, hPSC-treated spines demonstrated a high frequency of lumbar spinal fusion.

Evaluation of Spinal Fusion Using High-Resolution Micro-CT

Having demonstrated by manual palpation that hPSCs significantly enhance functional and mechanical stability, we next performed quantitative high-resolution micro-CT analyses. Three-dimensional reconstructions of the spines displayed large bilateral bone masses at level L4:L5 in hPSC-treated groups with bone bridging between adjacent transverse processes suggesting complete bony fusion (Fig. 2A). In contrast, the acellular control group demonstrated significantly reduced bone formation, as well as clear clefts between the two transverse processes, indicating incomplete fusion (Fig. 2A).

Next, micro-CT data analysis was performed to quantify the newly formed bone. hPSC-treated groups demonstrated a dose-dependent trend of increased bone mineral density (Fig. 2B). In hPSC-treated samples, the bone volume density (or bone volume/tissue volume) exhibited a statistically significant increase as compared with the acellular control group (Fig. 2C). In addition, hPSC-treated groups displayed a trend toward increased trabecular thickness (Fig. 2D) and a statistically significant dose-dependent increase in the trabecular bone number (Fig. 2E).

Evaluation of Biomechanical Properties Using Finite Element Analysis

Micro-CT analyses demonstrated that hPSC treatment induced robust bone formation; however, unlike ectopic bone formation and simple bone injury models, it is essential to test the biomechanical function in a spinal fusion model. Finite element analysis (FEA) revealed that hPSC treatment resulted in bilateral bone bridging with mechanical stress distributed evenly within a range of 0 (blue) to 10 (cyan) MPa (Fig. 3A). Contrastingly, stress distribution was concentrated to the small areas of bony bridge formation in the acellular control group. As a result, von Mises stress values exceeded the maximum stress bearing limit of 25 (Gy) MPa in the control group (Fig. 3A). Next, to assess bone strength within the newly formed bone, a randomly selected 2 mm × 2 mm × 2 mm cuboidal structure was isolated and evaluated by FEA for von Mises stress values (Fig. 3B). By both qualitative and qualitative parameters, all hPSC-treated groups exhibited decreased stress levels as compared with acellular control groups (Fig. 3C). In summary, biomechanical testing through finite element analysis further verified increased biomechanical stability and strength of spinal fusion in hPSC-implanted groups, in comparison with the acellular control group.

Evaluation of Bone Formation Using Histological and Immunohistochemical Analyses

To further explore the effects of hPSCs in promoting bone formation, histological analyses were performed by routine H&E and Masson's trichrome staining (Fig. 4A, 4B). The acellular control group showed decellularized cortical/cancellous bone chips (DBX material) in a predominantly hypocellular fibrous background, with minimal new-formed woven bone (Fig. 4A, 4B). In marked contrast, hPSC-treated groups depicted DBX material connected and contiguous with significant new-formed woven bone. Moreover, with escalating hPSC dosing, an increase in hypertrophic chondrocytes was observed indicative of active endochondral ossification (Fig. 4A, yellow arrows). Increased osteoid was also observed in a slight dose-dependent manner in hPSC-treated samples (Fig. 4B, green arrows). Further, histomorphometric quantification of bone area/total implant tissue area revealed significantly increased bone in hPSC-implanted samples as compared with the acellular control group, with a slight hPSC dose-dependent effect (Fig. 4C).

To confirm that hPSC-treatment induced increased endochondral bone formation, we performed immunostains for OCN, a late marker of osteogenesis. We observed that hPSC-treated samples exhibited a both significant and dose-dependent increase in OCN staining compared with acellular control (Fig. 4D). Additionally, we examined the efficiency of hPSC in promoting osteoblast and bone formation through BSP-positive staining. Once again, hPSC-treated groups showed significantly increased relative staining in a dose dependent manner (Fig. 4E).

Immunohistochemical staining for human-specific MHC (hMHC) confirmed that with increasing doses of hPSC application, increasing human antigen staining was observed (Fig. 5A). This was quantified as the number of hMHC-positive bone-lining osteoblasts and bone-resident osteocytes (Fig. 5C, 5D). These results showed that hPSC have a direct effect in new bone formation. Next, parallel staining was performed using rat-specific MHC (rMHC) (Fig. 5B). Similar to the pattern of hMHC expression, with increasing dosages of hPSC an increasing amount of rat-specific MHC staining was observed. When quantified, an increase in both rMHC positive, cuboidal, bone-lining osteoblasts and bone-resident osteocytes was observed with increasing dosages of hPSC (Fig. 5C, 5D). Notably, rat-specific osteoblasts outnumbered human-specific osteoblasts by a ratio of 3.9–10:1 (Fig. 5C).

©AlphaMed Press 2014

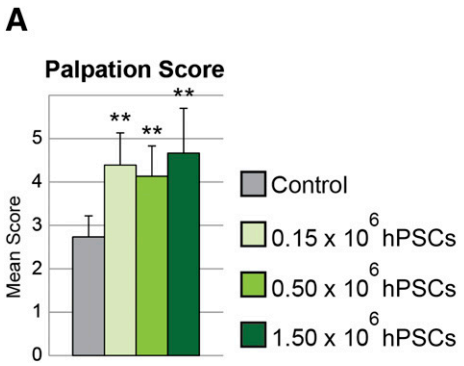

B

Treatment Group	Fusion Rate
Control	20%
0.15 x 10^6 hPSCs	100%**
0.50 x 10^6 hPSCs	80%**
1.50 x 10^6 hPSCs	100%**

Figure 1. Manual palpation. Acellular control was compared with three concentrations of hPSC-based bone graft substitutes. Spines were harvested 4 weeks postoperative and analyzed by manually applying flexion and extension forces against the L4/L5 vertebrae. **(A):** An average score of ≥4 was considered fused. **(B):** Fusion was apparent in 20% (1 of 5) of control-treated samples and 100% (6 of 6), 80% (4 of 5), and 100% (6 of 6) in 0.15×10^6, 0.50×10^6, and 1.50×10^6 hPSC-treated animals, respectively. **, $p \leq .01$ compared with control. No significant difference in fusion scores or rates was observed between hPSC-treated groups. Abbreviation: hPSC, human perivascular stem cell.

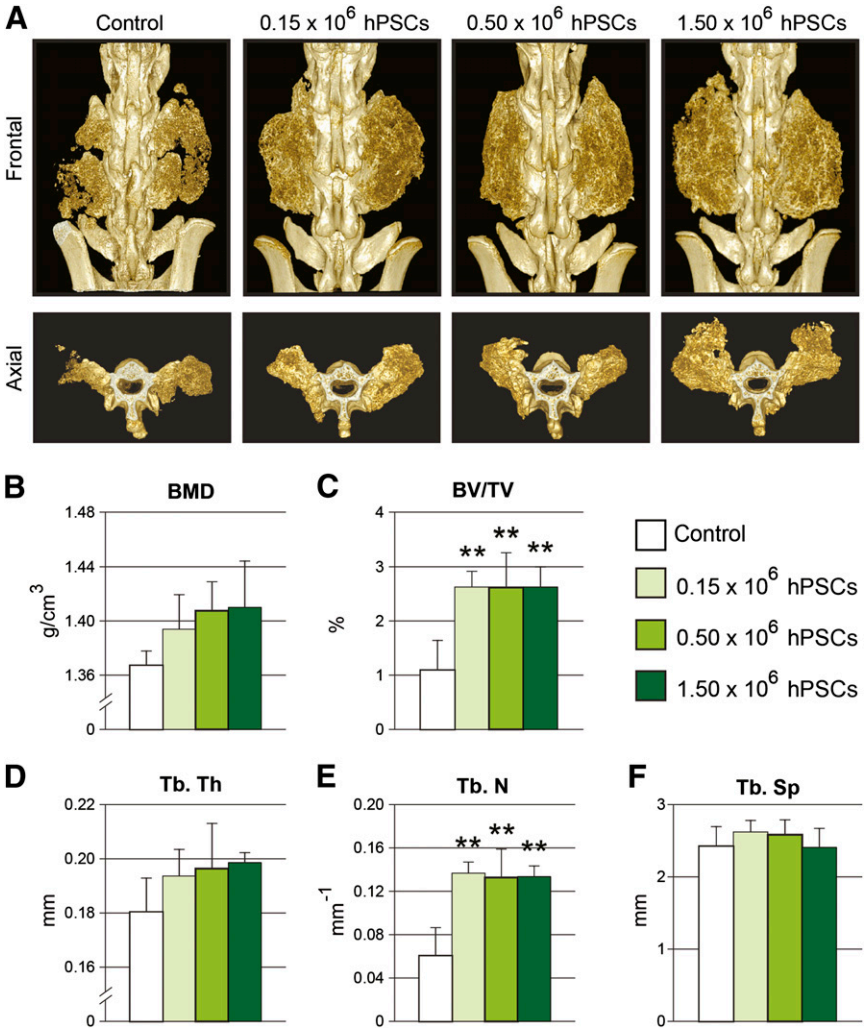

Figure 2. Micro-computed tomography (micro-CT) analysis. **(A):** Reconstructions of high-resolution micro-CT scans, shown in frontal and axial planes. **(B–F):** Micro-CT quantifications were next performed for bone mineral density **(B)**, fractional bone volume **(C)**, trabecular thickness **(D)**, trabecular number **(E)**, and trabecular spacing **(F)**. **, $p \leq .01$ compared with control. No significant difference in micro-CT parameters was observed between hPSC-treated groups. Abbreviations: BMD, bone mineral density; BV/TV, fractional bone volume; hPSC, human perivascular stem cell; Tb. N, trabecular number; TB. Sp, trabecular spacing; Tb. Th, trabecular thickness.

©AlphaMed Press 2014

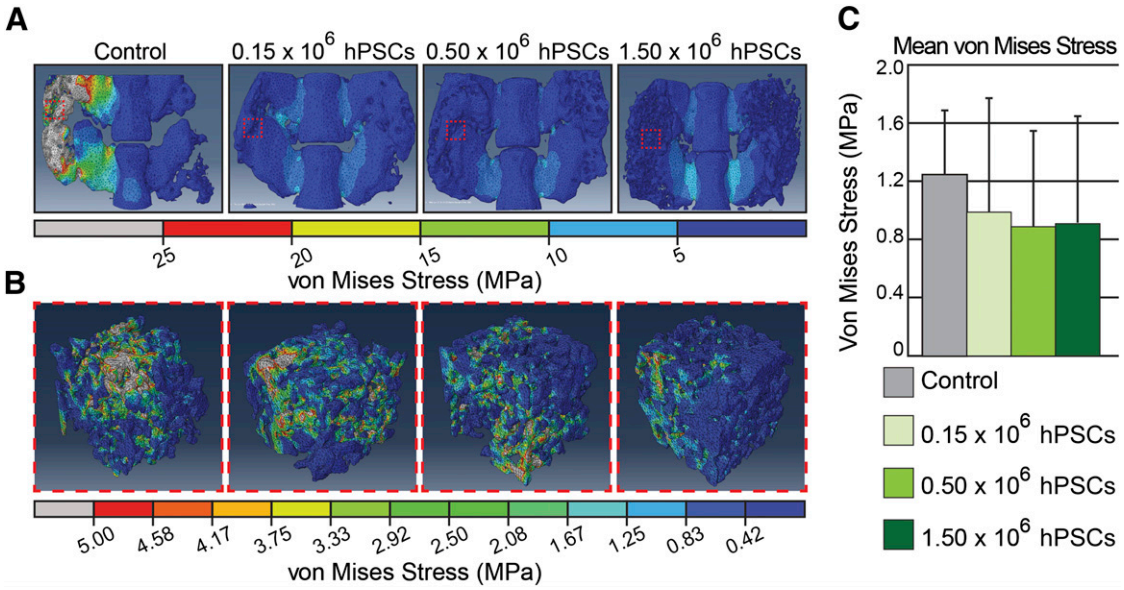

Figure 3. Biomechanical/finite element analysis. **(A):** A uniform compressive stress force of 0.5 MPa was applied on the superior surface of the L4/L5 spinal segment. (Gy scale bar indicates all values exceeding 25 MPa). **(B):** Cuboidal specimens from newly formed bone were next assessed for von Mises stress. **(C):** Quantification of cuboidal segments of newly formed bone for mean von Mises stress. Abbreviation: hPSC, human perivascular stem cell.

Likewise, rat-specific osteocytes outnumbered human-specific osteocytes by a ratio of 7.8–30.8:1 (Fig. 5D). Interestingly, a significant number of human-derived osteoblast and osteocytes persisted, indicating direct differentiation and incorporation into the bone matrix. Moreover, a significant dose-dependent effect was observed between hPSC treatment groups. Thus and in summary, immunohistochemistry for species-specific antigens verified that not only do hPSCs play a direct role in bone formation, but also hPSCs plays a role in paracrine support of host osteoprogenitor cell recruitment and/or differentiation.

Evaluation of the Matrix Deposition Using Histomorphometric Analysis

Finally, in vivo fluorescent dye labeling images were analyzed to investigate new matrix deposition. Double calcein injections were performed (with a 7-day interval between injections), revealing increased calcein labeling among hPSC-treated groups as well as clear double linear deposition in hPSC-treated groups (Fig. 6A). This was quantified, showing that hPSC-treated samples exhibited a dose-dependent increase in total calcein deposition (Fig. 6B). Next, two fluorescent dye labeling was performed, this time using calcein (green) and demeclocyline (orange), again with a time interval of 7 days. In hPSC-treated samples, a wide band of new-formed bone was apparent between green and orange labels (Fig. 6C, green and orange arrows). Overall, hPSC samples not only demonstrated increased bone formation but also increased active bone mineralization.

Discussion

Our data demonstrate that adipose-derived FACS-purified hPSCs delivered on a demineralized bone matrix scaffold—an osteoinductive matrix—can successfully induce functional bone tissue formation and reliable rat lumbar spinal. Prior to this study, evaluation of bone regeneration of hPSC were limited to nonfunctional bone regeneration models, including ectopic bone formation in a muscle pouch implant model [32] and reossification of calvarial bone defects [34]. Ectopic bone formation models are limited to validating in vivo osteogenic potential, and calvarial bone defects simply assess ossification and do not assess the functional properties of newly formed bone [44, 45]. In contrast, spinal fusion models provide a more clinically relevant assessment of the newly formed bone, including bone quantity and biomechanical strength.

Spinal fusion is one of the most common procedures performed to achieve stability in spinal disorders. As previously discussed, autogenous bone grafting, the gold standard of care for spinal fusion procedures, is limited in its use because of limited donor availability, additional surgical trauma and donor site morbidity [8–10]. Moreover, previously published rat spinal fusion studies assessing autologous bone grafting were observed to yield an inferior fusion rate when compared with hPSC treatment (0% fusion after 4 weeks and 11% fusion after 8 weeks with autologous bone grafting, compared with 80%–100% fusion in 4 weeks with hPSC treatment) [46, 47]. MSCs derived from multiple sources such as bone marrow and adipose tissue have attracted large interest for replacement of autogenous bone in spinal fusion procedures [48–52]. BMSCs, however, are limited in supply, and it is estimated that only 1 BMSC can be isolated per 100,000 cells [53]. To circumvent the shortage of MSCs, readily isolatable methods such as selective cell retention [54] and ex vivo cell culture methods have been developed [48–50]. Selective cell retention of osteoprogenitors are clinically available using Cellect Graft Preparation system (Dupuy, Raynham, MA, http://www.depuy.com); however, no clinical reports of success have been published [55]. Although ex vivo cell-cultured MSCs show promise toward successful spinal fusion rates ranging from 33% to 100% in animal studies [48–50, 56–58], extended processing time, additional cost, and risks of contamination are still limiting factors to its

©AlphaMed Press 2014

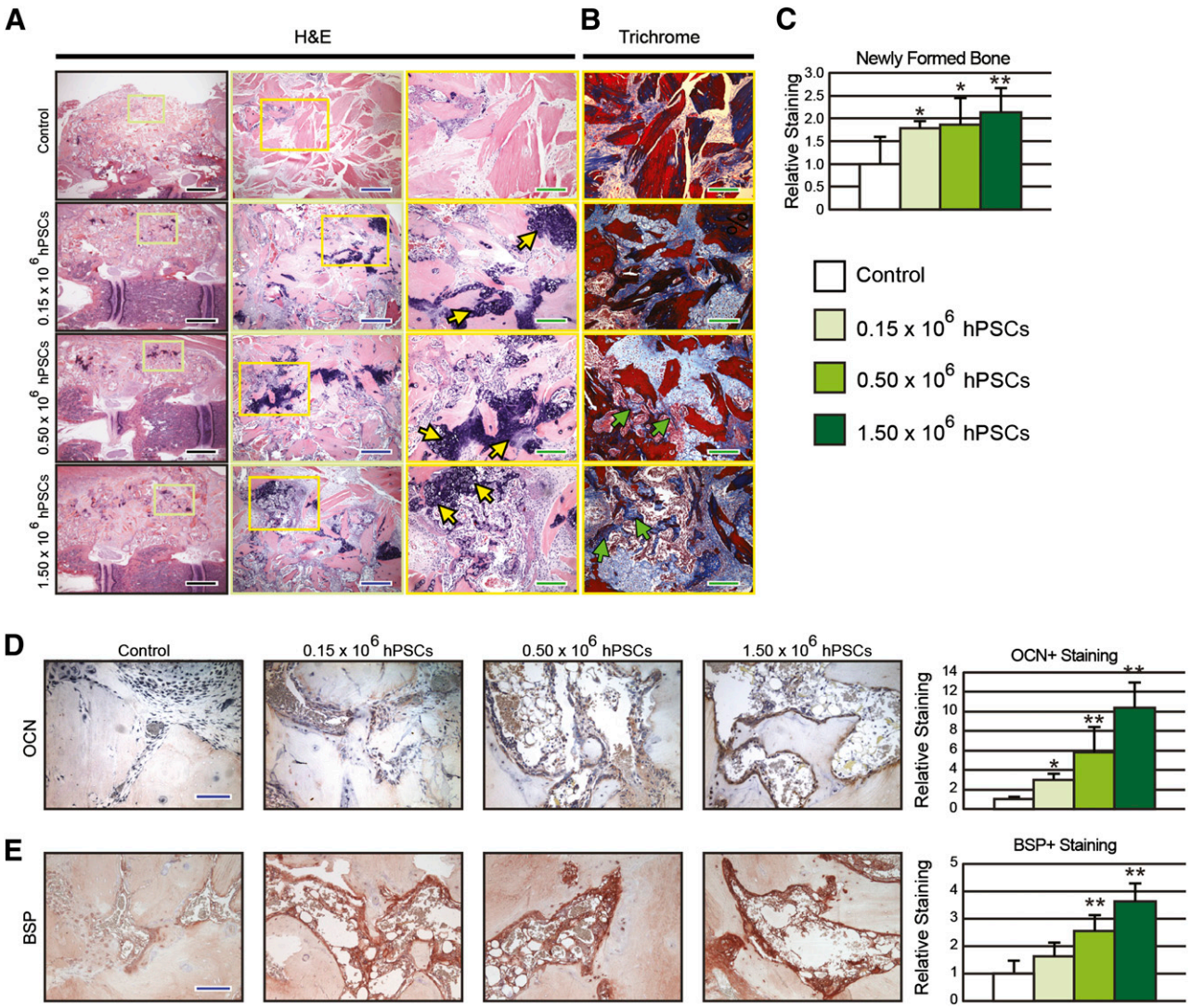

Figure 4. Histological analyses. **(A, B):** Coronal sections of spinal fusion stained with hematoxylin and eosin **(A)** and Masson's trichrome **(B)**. **(C):** Quantification for fractional bone area. **(D, E):** Representative osteocalcin **(D)** and bone sialoprotein, immunohistochemical staining, and quantification **(E)**. Yellow arrows = hypertrophic chondrocytes; green arrow = osteoid; black scale bar = 0.5 cm; blue scale bar = 100 μm; green scale bar = 50 μm. *, $p \leq .05$; **, $p \leq .01$ compared with control. A slight dose-dependent effect was observed in histomorphometric analysis between hPSC-treated groups. Abbreviations: BSP, bone sialoprotein; H&E, hematoxylin and eosin; hPSC, human perivascular stem cell; OCN, osteocalcin.

use. Similarly, although adipose-derived stem cells have been extensively studied in spinal fusion models with success [51, 59, 60], they possesses similar traits as BMSC in their culture dependency. Because PSCs are obtained from lipoaspirates and processed using FACS, a faster and contamination free source of osteoprogenitor cells can be obtained in comparison with bone marrow-derived MSCs.

Our data have partially elucidated the mechanisms underlying purified hPSC-mediated bone regeneration. Several possibilities have been proposed to explain the bone forming effects of hPSC. One explanation is the direct differentiation of hPSCs into osteoblasts. Chen et al. [61] have reported that pericytes undergo osteogenic differentiation in vitro, which has been subsequently verified in hPSCs [32, 33]. In the present study, we observed that hPSCs undergo direct differentiation into bone-forming cells via the detection of human antigen among both newly formed osteoblasts and osteocytes in vivo. Notably, however, the majority of osteoblasts and osteocytes were in fact of host rat origin.

This observation leads to the other likely possibility that hPSCs may not solely differentiate into bone-forming cells but may also lead to bone growth through predominantly trophic effects. For example, hPSCs may induce local chemotaxis and differentiation of osteoprogenitor cells, as well as neovascularization of the implant site, as documented in other MSC types [27, 33, 62–65]. Prior studies have shown that pericytes secrete significantly greater quantities of various growth factors in comparison with traditional MSC sources, including heparin growth factors, fibroblast growth factors (FGFs), and vascular endothelial growth factor [66]. These pro-osteogenic, provasculogenic growth factors have been observed in high quantities after in vivo implantation, in both intramuscular [33] and calvarial defect models [34]. In addition, previous studies have observed

 ©AlphaMed Press 2014

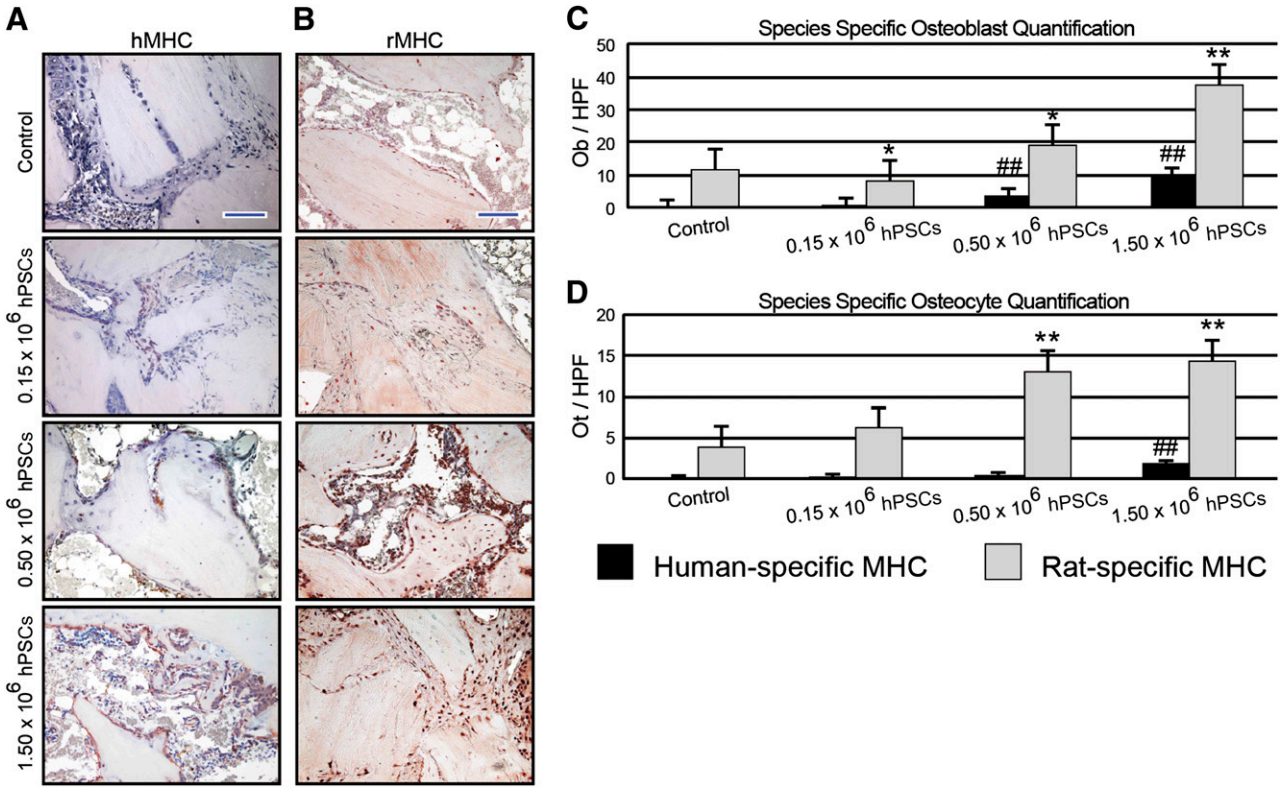

Figure 5. Species-specific MHC analyses. **(A, B):** Immunohistochemical staining of human- **(A)** or rat-specific **(B)** MHC. **(C, D):** Quantifications for osteoblasts **(C)** and osteocytes per higher power field **(D)**. Blue scale bar = 100 μm. $*$, $p \leq .05$ compared with rat-specific control values; $**$, $p \leq .01$ compared with rat-specific control values; ##, $p \leq .01$ compared with human-specific control values. A significant dose-dependent effect was observed between hPSC-treated groups. Abbreviations: hMHC, human-specific major histocompatibility complex; HPF, higher power field; hPSC, human perivascular stem cells; MHC, major histocompatibility complex; Ob, osteoblasts; Ot, osteocytes; rMHC, rat-specific major histocompatibility complex.

that growth factors such as FGFs have contributed to chemotaxis of stem cells [67–69]. In summary, although the mechanism by which hPSCs form bone is currently only partially understood, we have shown that the implanted hPSCs do not constitute the majority of bone-lining forming cells. This phenomenon has been frequently observed by other investigators and in other models of MSC implantation [70, 71]. Thus, PSCs have pleotropic functions to promote osteogenesis through both direct and indirect mechanisms along with supporting bone growth through increased vascularization.

Several recent studies have also expanded on the evolving relationship of perivascular progenitor cells to the cellular origin of MSCs within a microvascular environment. Currently, there now exists ample experimental proof that perivascular cells give rise in culture to mesenchymal stem cells [72], but the relevance of these observations to a possible natural role of perivascular cells as progenitors/regenerative cells in vivo is far less clear. The use of reporter mice has, however, recently brought evidence that perivascular cells—in particular pericytes—can act in situ as progenitors of white adipocytes [73], satellite cells and muscle fibers [74], follicular dendritic cells [75], and multiple other mesodermal cells [76]. Pericytes are also involved in myofibroblast generation and fibrosis development in the kidney, heart, and skeletal muscle [77]. Better understanding the functions of their native perivascular predecessors will allow further expansion of MSC application in tissue repair and wound healing.

Finally, our study has a number of limitations, which cautions extrapolation of our findings. For example, we evaluated three different dosages of hPSC application and found slight variation in dose dependency of cell seeding density. Markers of bone matrix deposition showed a slight dose-dependent increase between hPSC treatment groups, either by radiographic or histomorphometric analyses. In contrast, markers of osteoblastic differentiation showed a significant dose-dependent effect between hPSC treatment groups. Specifically, a strong dose-dependent effect was observed on rat osteoblast number, as well as species nonspecific markers. Thus, we can hypothesize that should a longer period of study be undertaken, a dose-dependent effect in bone matrix deposition and/or spinal fusion may be observed. Another limitation of our study was sample size (n = 5–6). Preliminary data yielded an anticipatory effect size of 2.0, suggesting that n = 5 would be sufficient for this study; however, this was observed to be slightly conservative. Thus, future studies will be planned to use a larger sample size and a longer study period to further investigate the dose-dependent effect of hPSC treatment.

Future studies must also be mindful of several intricacies in study design. Although the data presented herein possesses great promise, the current scientific standard for small animal spinal fusion assessment use healthy and young animals. Unfortunately, this model does not appropriately reflect the challenging clinical conditions of older populations requiring spinal fusion, who often

©AlphaMed Press 2014

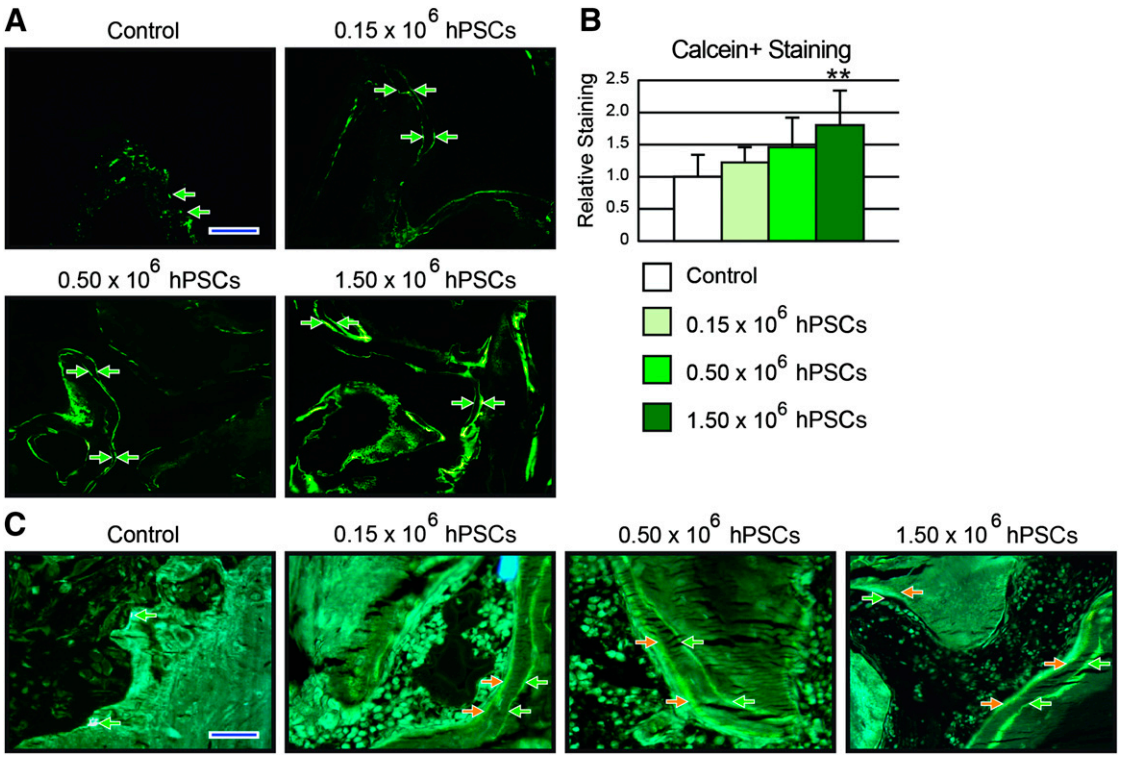

Figure 6. Bone labeling analyses. **(A):** Representative fluorescent microscopy pictures of calcein/calcein-labeled mineralization fronts of each treatment group. **(B):** Quantification of relative fluorescence of calcein/calcein mineralization fronts. **(C):** Representative fluorescent microscopy pictures of calcein/demeclocycline-labeled mineralization fronts. Green, calcein; orange, demeclocycline. A significant dose-dependent effect was observed in calcein staining between hPSC-treated groups. Abbreviation: hPSC, human perivascular stem cell.

possess an osteopenic/osteoporotic phenotype. As such, the use of ovariectomized or senile rodents may be required to test the true efficacy of experimental therapeutics. Additionally, to validate the findings presented herein, large animal studies will be necessary. Previous studies by Cui et al. [50] and Shamsul et al. [78] demonstrated the need to increase the number of MSCs administered when translating from small to large animal studies. For instance, when 2×10^6 BMSCs were implanted in rats, 100% fusion was observed [50]; however, to induce spinal fusion in sheep, hydroxyapatite seeded in $5–6 \times 10^7$ BMSCs was required [78]. This drastic increase in the number of cells required is directly related to increasing phylogenic complexity and as such will complicate clinical translation. Thus, future studies should seek to incorporate growth factors to increase osteogenic potency, reduce the number of PSCs or MSCs required, and ultimately optimize successful fusion for large animal studies and human application.

Conclusion

Our data demonstrate that hPSCs are a bipartite, readily isolated stem cell population capable of inducing rigid spinal fixation and robust bone formation. Compared with conventional stem cell populations with long culture periods, PSCs are isolated within a few hours using the FACS method. This procedure allows the whole process of retrieving hPSCs and implanting them to a defect to be performed within a single surgical procedure. Additionally, our prior studies have reported minimal variation in hPSC yields among different demographics, including age, gender, and body mass index. These pilot studies suggest that hPSCs can be isolated and used in bone regeneration across most donor patient conditions [34]. This lies in contrast to other traditional MSC sources [79, 80]. Lastly, the high homogeneity of hPSC populations can be advantageous in receiving future Food and Drug Administration approval, as a result of increased product characterization and uniformity of effect.

In summary, hPSCs show promise as a bipartite MSC population for future efforts in bone tissue engineering. In the present study, adipose-derived hPSCs were observed to be highly effective in inducing spinal fusion that was also able to withstand a load bearing weight. In future studies, we intend to extend our findings to clinically relevant large animal models.

Acknowledgments

This work was supported by California Institute for Regenerative Medicine Early Translational II Research Award TR2-01821 and National Institute of Arthritis and Musculoskeletal and Skin Diseases, NIH, Grant R01-AR061399-01A1.

Author Contributions

C.G.C.: conception and design, collection and/or assembly of data, data analysis and interpretation, manuscript writing; A.W.J.: conception and design, data analysis and interpretation, manuscript writing, final approval of manuscript; G.A. and L.C.: collection and/or assembly of data, data analysis and interpretation, manuscript writing; A.N. and R.L.: collection and/or assembly of

 ©AlphaMed Press 2014

data, data analysis and interpretation; K.L., G.B., and D.S.: collection and/or assembly of data; X.Z.: conception and design, data analysis and interpretation, final approval of manuscript; K.T., B.P., and C.S.: conception and design, financial support, administrative support, final approval of manuscript.

Disclosure of Potential Conflicts of Interest

K.T., B.P., and C.S. are inventors of perivascular stem cell-related patents filed from UCLA. K.T. and C.S. are founders of Scarless Laboratories Inc.

References

1 Yelin E, Callahan LF. The economic cost and social and psychological impact of musculoskeletal conditions. Arthritis Rheum 1995;38:1351–1362.

2 American Academy of Orthopaedic Surgeons. Burden of Musculoskeletal Diseases in the United States: Prevalence, Societal and Economic Cost. Rosemont, IL: American Academy of Orthopaedic Surgeons, 2008.

3 Deyo RA, Gray DT, Kreuter W et al. United States trends in lumbar fusion surgery for degenerative conditions. Spine 2005;30:1441–1445; discussion 1446–1447.

4 Gray DT, Deyo RA, Kreuter W et al. Population-based trends in volumes and rates of ambulatory lumbar spine surgery. Spine 2006;31:1957–1964.

5 Katz JN. Lumbar spinal fusion. Surgical rates, costs, and complications. Spine 1995;20 (suppl):78S–83S.

6 Lee CK, Langrana NA. A review of spinal fusion for degenerative disc disease: Need for alternative treatment approach of disc arthroplasty? Spine J 2004;4(suppl):173S–176S.

7 Taylor VM, Deyo RA, Cherkin DC et al. Low back pain hospitalization. Recent United States trends and regional variations. Spine 1994;19:1207–1213.

8 Mikhael MM, Huddleston PM, Nassr A. Postoperative culture positive surgical site infections after the use of irradiated allograft, nonirradiated allograft, or autograft for spinal fusion. Spine 2009;34:2466–2468.

9 Sawin PD, Traynelis VC, Menezes AH. A comparative analysis of fusion rates and donor-site morbidity for autogeneic rib and iliac crest bone grafts in posterior cervical fusions. J Neurosurg 1998;88:255–265.

10 Wolfe SA. Complications of harvesting cranial bone grafts. Plast Reconstr Surg 1996;98:567.

11 Deans RJ, Moseley AB. Mesenchymal stem cells: Biology and potential clinical uses. Exp Hematol 2000;28:875–884.

12 Minguell JJ, Conget P, Erices A. Biology and clinical utilization of mesenchymal progenitor cells. Braz J Med Biol Res 2000;33:881–887.

13 Schwartz RE, Reyes M, Koodie L et al. Multipotent adult progenitor cells from bone marrow differentiate into functional hepatocyte-like cells. J Clin Invest 2002;109:1291–1302.

14 Moerman EJ, Teng K, Lipschitz DA et al. Aging activates adipogenic and suppresses osteogenic programs in mesenchymal marrow stroma/stem cells: The role of PPAR-gamma2 transcription factor and TGF-beta/BMP signaling pathways. Aging Cell 2004;3:379–389.

15 Giannoudis P, Tzioupis C, Almalki T et al. Fracture healing in osteoporotic fractures: Is it really different? A basic science perspective. Injury 2007;38(suppl 1):S90–S99.

16 McIntosh K, Zvonic S, Garrett S et al. The immunogenicity of human adipose-derived cells: Temporal changes in vitro. Stem Cells 2006;24:1246–1253.

17 Meliga E, Strem BM, Duckers HJ et al. Adipose-derived cells. Cell Transplant 2007;16:963–970.

18 De Ugarte DA, Morizono K, Elbarbary A et al. Comparison of multi-lineage cells from human adipose tissue and bone marrow. Cells Tissues Organs 2003;174:101–109.

19 Aust L, Devlin B, Foster SJ et al. Yield of human adipose-derived adult stem cells from liposuction aspirates. Cytotherapy 2004;6:7–14.

20 Dahl JA, Duggal S, Coulston N et al. Genetic and epigenetic instability of human bone marrow mesenchymal stem cells expanded in autologous serum or fetal bovine serum. Int J Dev Biol 2008;52:1033–1042.

21 Niemeyer P, Kornacker M, Mehlhorn A et al. Comparison of immunological properties of bone marrow stromal cells and adipose tissue-derived stem cells before and after osteogenic differentiation in vitro. Tissue Eng 2007;13:111–121.

22 Paredes B, Santana A, Arribas MI et al. Phenotypic differences during the osteogenic differentiation of single cell-derived clones isolated from human lipoaspirates. J Tissue Eng Regen Med 2011;5:589–599.

23 Rajashekhar G, Traktuev DO, Roell WC et al. IFATS collection: Adipose stromal cell differentiation is reduced by endothelial cell contact and paracrine communication: Role of canonical Wnt signaling. Stem Cells 2008;26:2674–2681.

24 Meury T, Verrier S, Alini M. Human endothelial cells inhibit BMSC differentiation into mature osteoblasts in vitro by interfering with osterix expression. J Cell Biochem 2006;98:992–1006.

25 Crisan M, Yap S, Casteilla L et al. A perivascular origin for mesenchymal stem cells in multiple human organs. Cell Stem Cell 2008;3:301–313.

26 Crisan M, Chen CW, Corselli M et al. Perivascular multipotent progenitor cells in human organs. Ann N Y Acad Sci 2009;1176:118–123.

27 Crisan M, Corselli M, Chen CW et al. Multilineage stem cells in the adult: A perivascular legacy? Organogenesis 2011;7:101–104.

28 Crisan M, Deasy B, Gavina M et al. Purification and long-term culture of multipotent progenitor cells affiliated with the walls of human blood vessels: Myoendothelial cells and pericytes. Methods Cell Biol 2008;86:295–309.

29 Corselli M, Chen CW, Crisan M et al. Perivascular ancestors of adult multipotent stem cells. Arterioscler Thromb Vasc Biol 2010;30:1104–1109.

30 Corselli M, Chen CW, Sun B et al. The tunica adventitia of human arteries and veins as a source of mesenchymal stem cells. Stem Cells Dev 2012;21:1299–1308.

31 Zhang X, Péault B, Chen W et al. The Nell-1 growth factor stimulates bone formation by purified human perivascular cells. Tissue Eng Part A 2011;17:2497–2509.

32 James AW, Zara JN, Zhang X et al. Perivascular stem cells: A prospectively purified mesenchymal stem cell population for bone tissue engineering. Stem Cells Translational Medicine 2012;1:510–519.

33 Askarinam A, James AW, Zara JN et al. Human perivascular stem cells show enhanced osteogenesis and vasculogenesis with NELL-1 protein. Tissue Eng Part A 2013;19:1386–1397.

34 James A, Zara J et al. Stem Cells Translational Medicine 2012;1:673–684.

35 Li W, Lee M, Whang J et al. Delivery of lyophilized Nell-1 in a rat spinal fusion model. Tissue Eng Part A 2010;16:2861–2870.

36 Grauer JN, Patel TC, Erulkar JS et al. 2000 Young Investigator Research Award winner: Evaluation of OP-1 as a graft substitute for intertransverse process lumbar fusion. Spine 2001;26:127–133.

37 Parfitt AM, Drezner MK, Glorieux FH et al. Bone histomorphometry: Standardization of nomenclature, symbols, and units. J Bone Miner Res 1987;2:595–610.

38 Odgaard A, Linde F. The underestimation of Young's modulus in compressive testing of cancellous bone specimens. J Biomech 1991;24:691–698.

39 Keaveny TM, Pinilla TP, Crawford RP et al. Systematic and random errors in compression testing of trabecular bone. J Orthop Res 1997;15:101–110.

40 Zhu M, Keller TS, Spengler DM. Effects of specimen load-bearing and free surface layers on the compressive mechanical properties of cellular materials. J Biomech 1994;27:57–66.

41 Lu SS, Zhang X, Soo C et al. The osteoinductive properties of Nell-1 in a rat spinal fusion model. Spine J 2007;7:50–60.

42 Kuo CS, Hu HT, Lin RM et al. Biomechanical analysis of the lumbar spine on facet joint force and intradiscal pressure: A finite element study. BMC Musculoskelet Disord 2010;11:151.

43 Lee M, Li W, Siu RK et al. Biomimetic apatite-coated alginate/chitosan microparticles as osteogenic protein carriers. Biomaterials 2009;30:6094–6101.

44 Scott MA, Levi B, Askarinam A et al. Brief review of models of ectopic bone formation. Stem Cells Dev 2012;21:655–667.

45 Spicer PP, Kretlow JD, Young S et al. Evaluation of bone regeneration using the rat critical size calvarial defect. Nat Protoc 2012;7:1918–1929.

46 Koerner JD, Yalamanchili P, Munoz W et al. The effects of local insulin application to lumbar spinal fusions in a rat model. Spine J 2013;13:22–31.

47 Yuan W, James AW, Asatrian G et al. NELL-1 based demineralized bone graft promotes rat spine fusion as compared to commercially available BMP-2 product. J Orthop Sci 2013;18:646–657.

48 Gupta MC, Theerajunyaporn T, Maitra S et al. Efficacy of mesenchymal stem cell enriched grafts in an ovine posterolateral

lumbar spine model. Spine 2007;32:720–726; discussion 727.

49 Minamide A, Yoshida M, Kawakami M et al. The use of cultured bone marrow cells in type I collagen gel and porous hydroxyapatite for posterolateral lumbar spine fusion. Spine 2005;30:1134–1138.

50 Cui Q, Ming Xiao Z, Balian G et al. Comparison of lumbar spine fusion using mixed and cloned marrow cells. Spine 2001;26:2305–2310.

51 Lopez MJ, McIntosh KR, Spencer ND et al. Acceleration of spinal fusion using syngeneic and allogeneic adult adipose derived stem cells in a rat model. J Orthop Res 2009;27:366–373.

52 Miyazaki M, Zuk PA, Zou J et al. Comparison of human mesenchymal stem cells derived from adipose tissue and bone marrow for ex vivo gene therapy in rat spinal fusion model. Spine 2008;33:863–869.

53 Bruder SP, Jaiswal N, Ricalton NS et al. Mesenchymal stem cells in osteobiology and applied bone regeneration. Clin Orthop Relat Res 1998;;355(suppl):S247–S256.

54 Muschler GF, Matsukura Y, Nitto H et al. Selective retention of bone marrow-derived cells to enhance spinal fusion. Clin Orthop Relat Res 2005;432:242–251.

55 McLain RF, Fleming JE, Boehm CA et al. Aspiration of osteoprogenitor cells for augmenting spinal fusion: Comparison of progenitor cell concentrations from the vertebral body and iliac crest. J Bone Joint Surg Am 2005;87:2655–2661.

56 Wang T, Dang G, Guo Z et al. Evaluation of autologous bone marrow mesenchymal stem cell-calcium phosphate ceramic composite for lumbar fusion in rhesus monkey interbody fusion model. Tissue Eng 2005;11:1159–1167.

57 Kai T, Shao-qing G, Geng-ting D. In vivo evaluation of bone marrow stromal-derived osteoblasts-porous calcium phosphate ceramic composites as bone graft substitute for lumbar intervertebral spinal fusion. Spine 2003;28: 1653–1658.

58 Nakajima T, Iizuka H, Tsutsumi S et al. Evaluation of posterolateral spinal fusion using mesenchymal stem cells: Differences with or without osteogenic differentiation. Spine 2007; 32:2432–2436.

59 Zeng Q, Li X, Beck G et al. Growth and differentiation factor-5 (GDF-5) stimulates osteogenic differentiation and increases vascular endothelial growth factor (VEGF) levels in fat-derived stromal cells in vitro. Bone 2007;40: 374–381.

60 Hsu WK, Wang JC, Liu NQ et al. Stem cells from human fat as cellular delivery vehicles in an athymic rat posterolateral spine fusion model. J Bone Joint Surg Am 2008;90:1043–1052.

61 Chen CW, Corselli M, Peault B et al. Human blood-vessel-derived stem cells for tissue repair and regeneration. J Biomed Biotechnol 2012;2012:597439.

62 Feng J, Mantesso A, Sharpe PT. Perivascular cells as mesenchymal stem cells. Expert Opin Biol Ther 2010;10:1441–1451.

63 James AW, Zara JN, Corselli M et al. Use of human perivascular stem cells for bone regeneration. J Vis Exp 2012;63:e2952.

64 Tottey S, Corselli M, Jeffries EM et al. Extracellular matrix degradation products and low-oxygen conditions enhance the regenerative potential of perivascular stem cells. Tissue Eng Part A 2011;17:37–44.

65 Udani VM, Santarelli JG, Yung YC et al. Hematopoietic stem cells give rise to perivascular endothelial-like cells during brain tumor angiogenesis. Stem Cells Dev 2005;14:478–486.

66 Chen CW, Montelatici E, Crisan M et al. Perivascular multi-lineage progenitor cells in human organs: Regenerative units, cytokine sources or both? Cytokine Growth Factor Rev 2009;20:429–434.

67 Ozaki Y, Nishimura M, Sekiya K et al. Comprehensive analysis of chemotactic factors for bone marrow mesenchymal stem cells. Stem Cells Dev 2007;16:119–129.

68 Uchida K, Urabe K, Naruse K et al. Comparison of the cytokine-induced migratory response between primary and subcultured populations of rat mesenchymal bone marrow cells. J Orthop Sci 2007;12:484–492.

69 Ponte AL, Marais E, Gallay N et al. The in vitro migration capacity of human bone marrow mesenchymal stem cells: Comparison of chemokine and growth factor chemotactic activities. STEM CELLS 2007;25:1737–1745.

70 Oshima Y, Watanabe N, Matsuda K et al. Behavior of transplanted bone marrow-derived GFP mesenchymal cells in osteochondral defect as a simulation of autologous transplantation. J Histochem Cytochem 2005;53:207–216.

71 Oshima Y, Watanabe N, Matsuda K et al. Fate of transplanted bone-marrow-derived mesenchymal cells during osteochondral repair using transgenic rats to simulate autologous transplantation. Osteoarthritis Cartilage 2004; 12:811–817.

72 Murray IR, West CC, Hardy WR et al. Natural history of mesenchymal stem cells, from vessel walls to culture vessels. Cell Mol Life Sci 2014;71:1353–1374.

73 Tang W, Zeve D, Suh JM et al. White fat progenitor cells reside in the adipose vasculature. Science 2008;322:583–586.

74 Dellavalle A, Maroli G, Covarello D et al. Pericytes resident in postnatal skeletal muscle differentiate into muscle fibres and generate satellite cells. Nat Commun 2011;2:499.

75 Krautler NJ, Kana V, Kranich J et al. Follicular dendritic cells emerge from ubiquitous perivascular precursors. Cell 2012;150:194–206.

76 Olson LE, Soriano P. PDGFRβ signaling regulates mural cell plasticity and inhibits fat development. Dev Cell 2011;20:815–826.

77 Henderson NC, Arnold TD, Katamura Y et al. Targeting of αv integrin identifies a core molecular pathway that regulates fibrosis in several organs. Nat Med 2013;19:1617–1624.

78 Shamsul BS, Tan KK, Chen HC et al. Posterolateral spinal fusion with ostegenesis induced BMSC seeded TCP/HA in a sheep model. Tissue Cell 2014;46:152–158.

79 Oedayrajsingh-Varma MJ, van Ham SM, Knippenberg M et al. Adipose tissue-derived mesenchymal stem cell yield and growth characteristics are affected by the tissue-harvesting procedure. Cytotherapy 2006;8: 166–177.

80 Jurgens WJ, Oedayrajsingh-Varma MJ, Helder MN et al. Effect of tissue-harvesting site on yield of stem cells derived from adipose tissue: Implications for cell-based therapies. Cell Tissue Res 2008;332:415–426.

See www.StemCellsTM.com for supporting information available online.

 ©AlphaMed Press 2014